arXiv:cond-mat/0505593v1 [cond-mat.mtrl-sci] 24 May 2005

Fluctuation phenomena in crystal plasticity - a continuum model

Michael Zaiser§, Paolo Moretti

The University of Edinburgh, Institute for Materials and Processes, The King's Buildings, Sanderson Building, Edinburgh EH9 3JL, UK

Abstract. On microscopic and mesoscopic scales, plastic flow of crystals is characterized by large intrinsic fluctuations. Deformation by crystallographic slip occurs in a sequence of intermittent bursts ('slip avalanches') with power-law size distribution. In the spatial domain, these avalanches produce characteristic deformation patterns in the form of slip lines and slip bands which exhibit long-range spatial correlations. We propose a generic continuum model which accounts for randomness in the local stress-strain relationships as well as for long-range internal stresses that arise from the ensuing plastic strain heterogeneities. The model parameters are related to the local dynamics and interactions of lattice dislocations. The model explains experimental observations on slip avalanches as well as the associated slip and surface pattern morphologies.

Keywords: plasticity, fluctuations, defects, avalanches.

§ Tel. +44-131-6505671; Fax +44-131-6513470; e-mail M.Zaiser@ed.ac.uk

1. Introduction and Background

According to the classical paradigm of continuum plasticity, plastic deformation of crystalline solids resembles a smooth, quasi laminar flow process. This viewpoint has recently been challenged by experimental investigations which have demonstrated that, even in the absence of macroscopic deformation instabilities, plastic flow on microscopic and mesoscopic scales proceeds in a strongly heterogeneous and intermittent manner. Beyond the microscopic scale, where spatio-temporal localization of deformation is a trivial consequence of the discreteness of lattice defects (dislocations), slip localization phenomena extend over a wide range of mesoscopic scales and may involve the collective dynamics of very large numbers of defects. This is well known from the observation of slip lines or slip bands on the surface of deformed crystals (for an overview, see Neuhäuser, 1984), where slip steps on the surface manifest the collective motion of large numbers of dislocations. Recently, it has been shown that the spatial arrangement of 'slip events' has a fractal character (Weiss and Marsan, 2003). The consequences of a fractal distribution of slip on the surface morphology of plastically deformed crystals have been investigated by Zaiser et al. (2004), who demonstrated that the surface of plastically deformed Cu samples develops self-affine roughness over several orders of magnitude

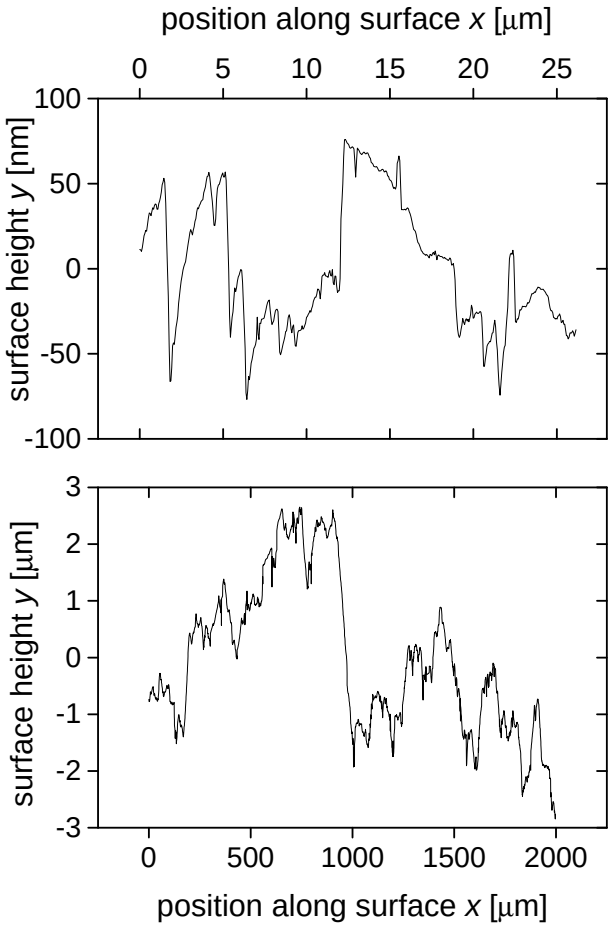

Figure 1. Surface profiles of a Cu polycrystal deformed in tension to a plastic strain $\epsilon = 9.6\%$. Top: AFM profile; bottom: SWLI profile. The x direction is parallel to the direction of the tensile axis. After Zaiser et al. (2004)

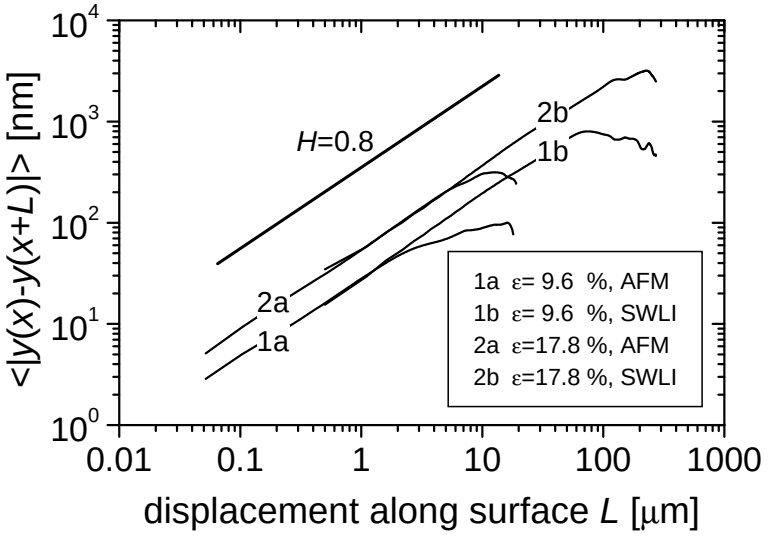

Figure 2. Roughness plots (mean height difference vs. distance along the profile) for AFM and SWLI profiles obtained at strains of 9.6 and 17.8 %. The corresponding profiles for $\epsilon = 9.6\%$ are shown in Figure 1.

in scale.

Spatio-temporal heterogeneity of slip in spite of macroscopically stable deformation is illustrated in Figures 1 and 2. Figure 1 shows surface profiles obtained from a Cu polycrystal with an initially flat surface after deformation to 9.6% tensile strain. The statistically self-affine nature of the profiles can be inferred by comparing profiles taken by Atomic Force Microscopy (AFM, profile length of 25 μm), and by Scanning White-Light Interferometry (SWLI, profile length 2 mm). Over several orders of magnitude, the self-affine behavior can be quantitatively characterized by a single Hurst exponent H as the average height difference $\langle |y(x) - y(x+L)| \rangle$ between two points on a profile increases as a function of their separation L like L^H with $H \approx 0.8$ (see Figure 2).

Information about the temporal dynamics of plastic flow can be inferred from acoustic emission measurements. Measurements on ice single crystals reported by Weiss and Grasso (1997) and Miguel et al. (2001) show temporal intermittency as the acoustic signal consists of a random sequence of discrete events ('slip avalanches'). These events exhibit a scale-free size distribution, as the probability density to observe events with energy release E decreases according to $p(E) \propto E^{-1.6}$ (Figure 3).

The present paper outlines a simple constitutive model that is capable of capturing spatial heterogeneity, temporal intermittency and scale-free behavior in plastic flow of crystals. To this end, we adopt concepts from the dynamics of random media by assuming that the deformation of a given volume element occurs through a random sequence of hardening and softening processes, such that the local flow stress is a fluctuating function of the local strain. Physically, these fluctuations result from randomness in the arrangement of the microstructural defects (dislocations) that produce the plastic deformation. Because of the crystalline nature of the medium, plastic deformation takes place by crystallographic slip, which in the present paper is assumed to occur on a single slip system only. Fluctuations in the local flow stress lead to shear strain fluctuations. These, in turn, give rise to long-range stress redistribution which can be expressed in terms of an elastic Green's function. Furthermore, dislocation-dislocation correlations give rise to a local back stress which can be expressed in terms of a second-order

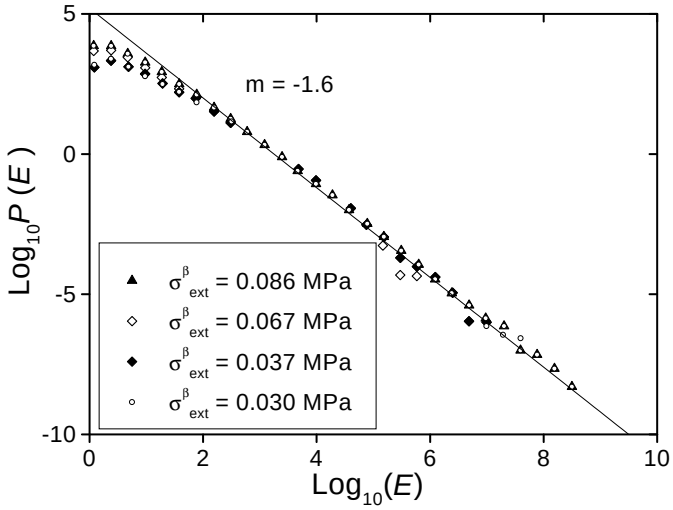

Figure 3. Distribution of energy releases in acoustic emission during creep deformation of ice single crystals; temperature T = 263 K, resolved shear stresses on the basal plane as indicated in the inset. After Miguel et al. (2001).

gradient of strain. These ideas are detailed in Section 2 where a stochastic plasticity model is presented. In Section 3, the numerical procedure employed to implement the model is briefly outlined. In Section 4, we discuss results obtained from the numerical simulations, and demonstrate that the model correctly accounts for the observed statistics of 'slip avalanches', the formation and arrangement of slip lines, and the corresponding deformation-induced surface morphology.

2. A Crystal Plasticity Model with Disorder

2.1. Basic structure of the model

We consider the simplest possible model for crystal plasticity with plastic deformation occurring by crystallographic slip on a single active slip system. Hence, the plastic distortion tensor is given by $\boldsymbol{\beta}^{\mathrm{p}}(\boldsymbol{r}) = \gamma(\boldsymbol{r})\boldsymbol{n} \otimes \boldsymbol{s}$ where γ is the shear strain on the slip system, and $\boldsymbol{n}$ and $\boldsymbol{s}$ are unit vectors pointing in the direction of the slip plane normal and the slip direction, respectively. In the following we assume without loss of generality that the slip direction corresponds to the x direction of a Cartesian coordinate system and the slip plane is the xz plane. The driving force for plastic flow is the shear stress $\sigma_{xy}(\boldsymbol{r}) =: \tau(\boldsymbol{r})$ acting in this slip system. We consider rate-independent elastic-plastic behavior. Hence, the stress acting in a volume element located at $\boldsymbol{r}$ must fulfill the inequality

$$\tau(\boldsymbol{r}) \leq \tau_{\mathrm{f}}(\boldsymbol{r}, \gamma(\boldsymbol{r})) \; . \tag{1}$$

Here τ_{f} is the local flow stress, which depends on internal state of the volume element under consideration. It is in general a function of the local strain $\gamma(\boldsymbol{r})$ and may also depend explicitly on the space coordinate $\boldsymbol{r}$. The stress $\tau(\boldsymbol{r}) = \tau_{\mathrm{ext}} + \tau_{\mathrm{int}}(\boldsymbol{r})$ acting from outside on the considered volume element is a sum of external and long-range internal stresses. The external stress, which acts as an external driving force on the system, is assumed space independent over the region of interest. The space-dependent internal stress field $\tau_{\mathrm{int}}(\boldsymbol{r})$ is a functional of the (in general spatially non-homogeneous) strain field $\gamma(r)$; it vanishes for a homogeneous deformation state.

If the inequality (1) is violated, the local strain $\gamma(\boldsymbol{r})$ increases quasi-instantaneously until Eq. (1) is again satisfied. Impossibility to satisfy this equation implies ductile failure of the system.

2.2. Evaluation of long-range internal stresses

We calculate the internal stresses in an infinite three-dimensional body with an arbitrary plastic distortion field $\boldsymbol{\beta}^{\mathrm{p}}(\boldsymbol{r})$. The external stress is assumed to be zero. (A non-zero external stress simply adds to the internal stresses.) We start out from the elastic equilibrium equation for the components σ_{ij} of the stress tensor:

$$-\partial_j \sigma_{ij} = f_i \ , \tag{2}$$

where f_i are the body forces and sums are performed over repeated indices. The above equation can be rewritten in terms of the components u_i of the elastic displacement vector as

$$-\partial_j C_{ilkl} \partial_k u_l = f_i, \tag{3}$$

where C_{ijkl} are components of Hooke's tensor. The solution of Equation (3) has the form

$$u_i(\mathbf{r}) = \int \Gamma_{ik}(\mathbf{r}-\mathbf{r}') f_k(\mathbf{r}') d^3 r' \tag{4}$$

where the Fourier transform of the elastic Green's tensor $\Gamma_{ik}(\mathbf{r})$ is $\tilde{\Gamma}_{ik}(\mathbf{k}) = [-C_{ijkl} k_j k_l]^{-1}$.

We now first consider the particular problem of a plastically deformed 'inclusion' where the plastic distortion has a constant value β^{p} over a certain volume V and is zero elsewhere. This *inclusion problem* is solved as follows: The volume V is first cut out of the surrounding matrix and deformed plastically in order to produce a stress-free strain β^{p}. To re-insert it into the matrix, interface tractions are applied, such that the original shape is restored. According to Equation (2) these interface tractions are

$$f_i = C_{ijkl} \beta^{\mathrm{p}}_{kl} \partial_j H_V(\mathbf{r}), \tag{5}$$

where the function $H_V(\mathbf{r})$ is equal to unity within V and zero elsewhere. The volume is then placed in its original position and relaxed. Elastic relaxation proceeds until the tractions produced by the relaxation strain β^{r} balance those given by Equation (5). The Fourier transform of the corresponding displacement field is

$$u^r_i(\mathbf{k}) = i \Gamma_{ik}(\mathbf{k}) C_{klmn} \beta^{\mathrm{p}}_{mn} k_l H_V(\mathbf{k}) \ .. \tag{6}$$

The total elastic distortion is then the sum of the relaxation strain and the initial distortion $-\beta^{\mathrm{p}}_{ij} H_V(\mathbf{r})$ applied to "restore" the original shape before relaxation. The associated total stress reads $\sigma_{ij}(\mathbf{r}) = C_{ijkl}(\beta^{\mathrm{r}}_{kl} - \beta^{\mathrm{p}}_{kl} H_V(\mathbf{r}))$ and its Fourier transform is

$$\sigma_{ij}(\mathbf{k}) = -C_{ijlm} \left(k_m k_o \tilde{\Gamma}_{ln}(\mathbf{k}) C_{nopq} + \frac{1}{9} \delta_{lp} \delta_{mq} \right) \beta^{\mathrm{p}}_{pq} \tilde{H}_V \ . \tag{7}$$

The angular average

$$\tilde{\Gamma}^0_{ijlm} = \frac{1}{4\pi} \int C_{ijno} [k_o k_q \tilde{\Gamma}_{np}(\mathbf{k}) C_{pqlm} + \frac{1}{9} \delta_{ln} \delta_{mo}] d\Omega \tag{8}$$

does not depend on the modulus k of the wavevector since $\tilde{\Gamma}_{np}$ scales like k^{-2}. The stress hence can be written as

$$\sigma_{ij}(\mathbf{k}) = [-\tilde{\Gamma}^0_{ijlm} + \tilde{\Gamma}^*(\mathbf{k}/k)] \beta^{\mathrm{p}}_{lm} H_V(\mathbf{k}) \ , \tag{9}$$

where the second term is simply defined by $\tilde{\Gamma}^*(\mathbf{k}/k) = C_{ijno}[k_o k_q \tilde{\Gamma}_{np}(\mathbf{k}) C_{pqlm} + \frac{1}{9}\delta_{ln}\delta_{mo}] - \tilde{\Gamma}^0_{ijlm}$.

The above procedure can be straightforwardly generalized for an arbitrary distribution of the plastic distortion $\beta^{\mathrm{p}}(\mathbf{r})$ by considering each volume element as a separate "inclusion". Equation (9) becomes

$$\sigma_{ij}(\mathbf{k}) = [-\tilde{\Gamma}^0_{ijlm} + \tilde{\Gamma}^*(\mathbf{k}/k)]\beta^{\mathrm{p}}_{lm}(\mathbf{k}) \tag{10}$$

and, in real space,

$$\sigma_{ij}(\boldsymbol{r}) = -\tilde{\Gamma}^0_{ijlm}\beta^{\mathrm{p}}_{lm}(\mathbf{r}) + \int \Gamma^*(\mathbf{r}-\mathbf{r}')\beta^{\mathrm{p}}_{lm}(\mathbf{r}')d^3r' \; . \tag{11}$$

The non-local kernel $\Gamma^*(\mathbf{r}-\mathbf{r}')$ is the inverse Fourier transform of $\tilde{\Gamma}^*(\mathbf{k}/k)$; it scales like $1/r^3$ and it can be shown that it has zero angular average. What has been done so far holds for strain fields that go to zero at infinite distances. If the asymptotic value of the plastic strain assumes a non-zero value $\beta^{\mathrm{p},\infty}$, we have to add the corresponding stress-free strain as follows:

$$\sigma_{ij}(\mathbf{k}) = \tilde{\Gamma}^0_{ijlm}[\beta^{\mathrm{p},\infty}_{lm} - \beta^{\mathrm{p}}_{lm}(\mathbf{r})] + \int \Gamma^*(\mathbf{r}-\mathbf{r}')\beta^{\mathrm{p}}_{lm}(\mathbf{r}')d^3r'. \tag{12}$$

For a plastic distortion field which has the *average* value $\langle\beta^{\mathrm{p}}\rangle$, the asymptotic value $\beta^{\mathrm{p},\infty}$ is replaced by the average $\langle\beta^{\mathrm{p}}\rangle$ since the fluctuation contributions average out if integrated over the infinite contour. Hence, the internal stress can be envisaged as the sum of a mean-field contribution and a non-local term with a kernel of zero angular average. For the purpose of a depinning theory built with this type of non-local elastic interaction, one may note that in Fourier space the kernel scales like k^a with $a = 0$, i.e., mean-field theory is expected to be valid in all dimensions.

For later use we give explicit expressions for the case where the plastic strain is determined by slip on a single slip system, $\boldsymbol{\beta}^{\mathrm{p}} = \gamma(\boldsymbol{r})\mathrm{e}_y \otimes \mathrm{e}_x$, and the shear strain γ depends on the x and y coordinates only. (Such a quasi-two-dimensional model corresponds to a system of straight parallel edge dislocations, cf. below.) In this case, the internal shear stress $\tau_{\mathrm{int}} = \sigma_{xy}$ is in Fourier space given by

$$\langle\tau_{\mathrm{int}}(\boldsymbol{k})\rangle = -\frac{G}{\pi(1-\nu)}\gamma(\boldsymbol{k})\frac{k_x^2k_y^2}{|\boldsymbol{k}|^4} \; , \tag{13}$$

and in real space by

$$\begin{aligned}\langle\tau_{\mathrm{int}}(\boldsymbol{r})\rangle = {} & \frac{G}{2\pi(1-\nu)}\int \gamma(\boldsymbol{r}')\left[\frac{1}{(\boldsymbol{r}-\boldsymbol{r}')^2} - \frac{8(x-x')^2(y-y')^2}{(\boldsymbol{r}-\boldsymbol{r}')^6}\right]\mathrm{d}^2\boldsymbol{r}' \\ & + \frac{G}{4(1-\nu)}[\langle\gamma\rangle - \gamma(\boldsymbol{r})] \; .\end{aligned} \tag{14}$$

Here, G is the shear modulus and ν the Poisson's ratio. From these expressions, two points may be noted: (i) The elastic kernel is not positively definite in real space. (ii) There exist certain space-dependent strain fluctuations (fluctuations with wavevectors in the x and y directions) which do not give rise to any long-range internal stresses. The implications of this will be discussed below.

2.3. Dislocation-related stresses and internal-stress fluctuations

We now discuss the physical origin of the 'flow stress' $\tau_{\mathrm{f}}(\boldsymbol{r},\gamma)$. On the microscopic scale, plastic flow of a crystal is brought about by the motion of linear lattice defects (dislocations). The flow stress of a small mesoscopic volume (a volume containing multiple dislocations/dislocation segments) corresponds to the stress required to move dislocations through the stress 'landscape' within this volume. In the absence of other defects, this 'landscape' is created by the

dislocations themselves. The resulting flow stress $\tau_{\rm f} = \delta\tau + \tau_{\rm p}$ can be envisaged as a sum of two contributions [for a more detailed discussion, see Zaiser and Seeger (2002), Groma, Csikor and Zaiser (2003), Zaiser and Aifantis (2005)]:

(i) A spatially fluctuating stress $\delta\tau(\boldsymbol{r})$ which depends on the positions of the individual dislocations. The average of the fluctuating stress is zero, and the characteristic 'amplitude' of the fluctuations is given by

$$\langle \delta\tau(\boldsymbol{r})^2 \rangle = K^2 G^2 b^2 \rho(\boldsymbol{r}) \; , \tag{15}$$

where $K^2 = \ln(\xi/b)/[8\pi(1-\nu)^2]$ is a numerical constant of the order of unity which depends on the elastic properties of the crystal lattice, and logarithmically on the characteristic range $\xi \approx 1/\sqrt{\rho}$ of dislocation-dislocation correlations. The spatial correlation function of the fluctuating internal stress field is given by

$$\langle \delta\tau(\boldsymbol{r}) \delta\tau(\boldsymbol{r}+\boldsymbol{r}') \rangle = \langle \delta\tau(\boldsymbol{r})^2 \rangle h(\boldsymbol{r}'/\xi) \; , \tag{16}$$

where $h(\boldsymbol{r}'/\xi)$ is a short-range correlation function with characteristic range $\xi \approx 1/\sqrt{\rho}$ (Zaiser and Seeger, 2002).

Dislocation glide increases the local strain and modifies the fluctuating stresses within the surrounding mesoscopic volume element. In the absence of detailed information about the individual dislocation positions, we take this evolution of the stress 'landscape' into account by envisaging the fluctuating stress as a random function not only of space but also of *strain*, with the correlation function

$$\langle \delta\tau(\boldsymbol{r},\gamma) \delta\tau(\boldsymbol{r}+\boldsymbol{r}',\gamma+\gamma') \rangle = \langle \delta\tau(\boldsymbol{r})^2 \rangle h(\boldsymbol{r}'/\xi) g(\gamma/\gamma_{\rm corr}) \; , \tag{17}$$

where g is another short-range function. The 'correlation strain' $\gamma_{\rm corr}$ can be estimated as the local strain produced when all dislocations in a volume element move by the distance ξ, $\gamma_{\rm corr} = \rho b \xi \approx b\sqrt{\rho}$.

(ii) If small groups of dislocations move in a correlated manner, their mutual interactions tend to homogenize deformation in the slip plane. This can be described by a 'pile-up stress' $\tau_{\rm p}(\boldsymbol{r})$ which can be approximated by a second-order gradient of the strain according to

$$\tau_{\rm p}(\boldsymbol{r}) = \frac{DG}{\rho}\gamma_{xx} \quad (d=2) \; , \quad \tau_{\rm p}(\boldsymbol{r}) = \frac{DG}{\rho}[\gamma_{xx}+\gamma_{zz}] \quad (d=3) \; . \tag{18}$$

Here, ρ is the total dislocation density and D a constant of the order of unity [see Groma, Csikor and Zaiser (2003)]. In Eq. (18), $d \in [2,3]$ is the dimensionality of the model. The first expression ($d=2$) refers to the special case where deformation is due to the motion of straight edge dislocations, such that the shear strain γ depends on the x and y coordinates only.

2.4. Strain hardening

During deformation, the dislocation density often increases with increasing strain, leading to an increase of the stress required to sustain plastic flow (strain hardening). In our model we may take this into account in two manners:

(a) We explicitly account for the strain evolution of the dislocation density ρ. In the simplest case, this is given by [see e.g. Zaiser (1998)]

$$\partial_t \rho = \frac{\beta}{b}\sqrt{\rho}\dot{\gamma} \quad , \quad \rho(\gamma) = \left(\frac{\beta\gamma}{2b}\right)^2 \; , \tag{19}$$

where $\beta \approx 0.02$ is a small non-dimensional parameter. It follows that the dislocation density is approximately constant over the 'correlation strain' $\gamma_{\rm corr} \approx b\sqrt{\rho}$ but increases slowly over larger

strain intervals. This leads to a corresponding increase of the amplitude of the fluctuating stress $\delta\tau(\boldsymbol{r},\gamma)$, which scales in proportion with the local strain $\gamma(\boldsymbol{r})$.

(b) In phenomenological hardening theories, hardening is often described by a strain dependent 'back stress' which is subtracted from the locally acting stress. In the simplest case of linear strain hardening, this stress is given by $\tau_{\rm b} = -\Theta\gamma$ where Θ is the hardening coefficient. If we choose this description of hardening, we keep the amplitude of the fluctuating stresses constant but subtract a slowly increasing back stress which is proportional to the local strain.

Actually, both descriptions yield very similar results. As discussed in the next paragraph, our equations have the structure of an elastic manifold depinning model, with the fluctuating stress $\delta\tau$ acting as a random pinning field. Since the pinning stress in such models is governed by the negative maxima of the pinning field, a linear increase of the amplitude of the pinning field with increasing strain, or the subtraction of a strain-dependent back stress, both have the same consequence: The stress required to overcome these maxima increases linearly as a function of the local strain.

2.5. Plastic flow and elastic manifold depinning

Collecting all stress contributions discussed in Sections above, we find that plastic flow occurs (γ increases quasi-instantaneously) as soon as the inequality

$$\tau_{\rm ext} + \tau_{\rm int}(\boldsymbol{r}) + \frac{DG}{\rho}[\gamma_{xx} + \gamma_{yy}] + \delta\tau(\boldsymbol{r},\gamma) \leq 0 \tag{20}$$

is violated. The asymptotic behavior of this model for positive external stresses corresponds to that of the equation of motion

$$\frac{1}{B}\partial_t\gamma(\boldsymbol{r}) = \tau_{\rm ext} + \tau_{\rm int}(\boldsymbol{r}) + \frac{DG}{\rho}[\gamma_{xx} + \gamma_{yy}] + \delta\tau(\boldsymbol{r},\gamma)\ . \tag{21}$$

in the rate-independent limit $B \to \infty$. Formally, Eq. (21) can be envisaged as describing the overdamped dynamics of an elastic manifold with coordinates $(\gamma, \boldsymbol{r})$ which moves in the γ-direction through a random medium. In the two-dimensional case where $\gamma = \gamma(x, y)$ depends only on the x and y coordinates ($d = 2$), our model may be considered a continuum approximation of a quasi-two-dimensional system of straight parallel dislocations. If the strain depends on all three spatial coordinates, and the model mimics the large-scale behavior of a system of three-dimensionally curved dislocations. In either case, the model can be formally envisaged as describing the motion of a d-dimensional elastic manifold through a disordered $d + 1$-dimensional medium which exerts a fluctuating pinning force $\delta\tau$. Due to the infinite range of the interaction kernel governing the internal stress $\tau_{\rm int}(\boldsymbol{r})$, one expects the second-order gradient term in Eqs. (20,21) to be irrelevant for the large-scale behavior, and the model exhibits mean-field behavior irrespective of the dimensionality of the 'manifold'.

Two differences may be noted with respect to conventional models of elastic manifold depinning: (i) If we account for hardening, either the mean value or the amplitude of the pinning field increases as the manifold advances, i.e., we are dealing with a net 'uphill' motion of the manifold. The consequences of this will be discussed in Section 4.2. (ii) As can be directly seen from Eq. (14), the elastic kernel mediating the long-range interaction is not positively definite. Hence, the 'no passing'-theorem (Middleton 1992) need not hold and the existence of a unique depinning threshold is not a priori guaranteed. In spite of these caveats, numerical investigation of the model shows depinning-like behavior, as demonstrated in Section 4.

3. Numerical Implementation

For numerical implementation of the model we focus on the two-dimensional case. (Because of the mean-field nature of the long-range interactions, a generalization to three dimension is not expected to make any significant difference). We use a lattice automaton model where we discretize space in terms of a two-dimensional array of cells, each cell representing a mesoscopic volume element whose edge length $l \approx \xi$ is of the order of the correlation length of the stress fluctuations. Accordingly, the fluctuating stresses in different volume elements are assumed as statistically independent random variables. In a similar spirit, the local strains are discretized in units of the correlation strain $\gamma_{\rm corr} \approx b\sqrt{\rho}$, and the fluctuations at different strain steps are considered statistically independent. A bulk system is mimicked by imposing periodic boundary conditions in both directions. The total dislocation density ρ and, hence, the statistical properties of the fluctuating internal stress field are assumed spatially homogeneous. A non-dimensional and dislocation density independent formulation is achieved by scaling all lengths in proportion with $\xi \approx 1/\sqrt{\rho}$, all stresses in proportion with $KGb\sqrt{\rho}$, and all strains in proportion with $b/\xi \approx b\sqrt{\rho}$.

The procedure for implementing the random function $\delta\tau(\gamma, \boldsymbol{r})$ in Eq. (20) is here discussed in the absence of hardening. To each cell we assign initially a negative random value of $\delta\tau$ drawn from the negative half of a Gaussian distribution with unit variance [Eq. (3)]. This ensures that there is no plastic flow at zero external stress; in physical terms, it implies that initially all dislocations are trapped in configurations where they are held up by negative (back) stresses. Whenever the strain within a cell increases, we assign a new (positive or negative) random value of $\delta\tau$ to this cell, which we draw again from a Gaussian distribution of unit variance. We note in passing that the Gaussian shape of the probability distribution of $\delta\tau$ is not crucial; other distributions with finite first and second moments produce similar results.

In each simulation we increase the applied stress $\tau_{\rm ext}$ from zero in small increments $\Delta\tau_{\rm ext}$. After a stress increment we check for all volume elements whether Eq. (20) is violated. In all volume elements where this happens, we increase the local strains by a unit amount and assign new values of $\delta\tau$. After this simultaneous update procedure is completed , we compute the internal stress field $\langle\tau_{\rm int}(\boldsymbol{r})\rangle$ corresponding to the new strain pattern by using the periodically continued elastic Green's function of a two-dimensional isotropic medium, Eq. (14), and evaluate the gradient-dependent stress contribution using the discrete second-order gradient. Once the new internal stresses are computed, we check again for all volume elements whether Eq. (20) is now satisfied and, if not, increase the local strains etc.. The process is repeated until the local stress everywhere falls below the local yield stress, or until the average strain within the system exceeds a prescribed maximum value at which we terminate our simulation. If the system settles into an equilibrium configuration before reaching the terminal strain, we increase the external stress further by $\Delta\tau_{\rm ext}$, and so on. This procedure implements an adiabatically slow drive, provided that the external stress increment $\Delta\tau_{\rm ext}$ is chosen small enough (the practical criterion being simply that the results do not change if the stress increment is further decreased).

4. Results and Discussion

4.1. Stress-strain characteristics and avalanche dynamics in the absence of hardening

We first study the model in the absence of hardening. Then, the 'pinning stress' $\delta\tau$ has stationary stochastic properties. A stress-strain graph obtained for this case is illustrated in

Figure 4. The calculation has been done for the following parameters typical for the onset of deformation of Cu single crystals: $G = 40000$ MPa, $\nu = 0.3$, $b = 2.5 \times 10^{-10}$m, $\rho = 10^{12}$ m^{-2}, and $\xi = 1/\sqrt{\rho} = 10^{-6}$m. With these parameters, $K \approx 1$, while the parameter D in Eq. (18) was chosen as $D = 0.1$. We note that, in the context of the present model, this latter term mainly serves to break the symmetry which exists in the elastic kernel given by Eq. (14) between the directions in and out of the slip plane. The numerical value of D is of little influence on our results unless very high D values are assumed.

From Figure 4, the following observations can be made: (i) In spite of the fact that the averages of $\delta\tau$ over γ at fixed $\boldsymbol{r}$ (or over $\boldsymbol{r}$ at fixed γ) are zero, a finite stress (yield stress) of $\tau_c \sim 0.4$ (in scaled coordinates) is required to sustain deformation. This is because at low applied stresses the system becomes pinned in configurations where the fluctuating stress $\delta\tau$ is negative in most volume elements, thereby creating a non-zero average back stress. (ii) The yield stress is approached asymptotically through a 'microplastic' region where such metastable configurations are gradually eliminated. (iii) The increase of plastic strain with increasing stress occurs in discrete 'slip avalanches' of varying size. These avalanches are visible as steps on the stress-strain curves, which assume a staircase-like shape. The intervals between the larger avalanches divide into avalanches of smaller size, and the characteristic avalanche size diverges as one approaches the yield stress. In dimensional units, the scaled stress and strain ranges visible in Figure 4 correspond to $0 \leq \tau_{\rm ext} \leq 5$ MPa and $0 \leq \langle\gamma\rangle \leq 0.5\%$, respectively. The figure can, hence, be thought of as describing the microplastic region and yielding transition at the onset of easy-glide deformation of a fcc single crystal. We also note that the dimensional yield stress obeys Taylor's well-established scaling relation $\tau_c = \alpha G b\sqrt{\rho}$. The numerical value of $\alpha \approx 0.4$ obtained from the simulation is within the characteristic range $0.2 < \alpha < 0.5$ observed in experiment.

We first study the *average* behavior of our model. By averaging the stress-strain graphs over a large number of simulations, we obtain a (nearly) smooth stress-strain relationship (Figure 5). The average strain diverges as the stress approaches the yield stress τ_c. A semi-logarithmic plot of γ vs. $\tau_c - \tau_{\rm ext}$ reveals that this divergence is logarithmic in nature.

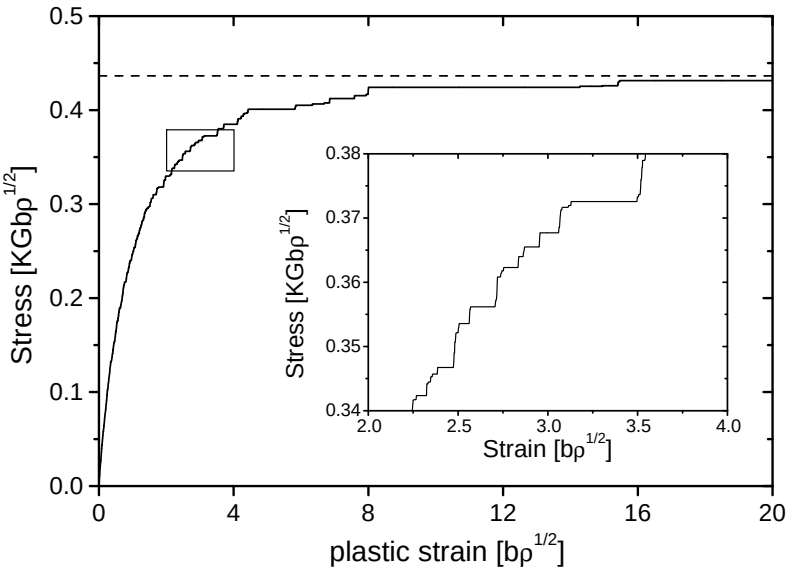

Figure 4. Stress-strain curve as obtained from simulation of a system with 128×128 sites; dashed line: critical stress τ_c; Insert: detail of the same stress-strain graph.

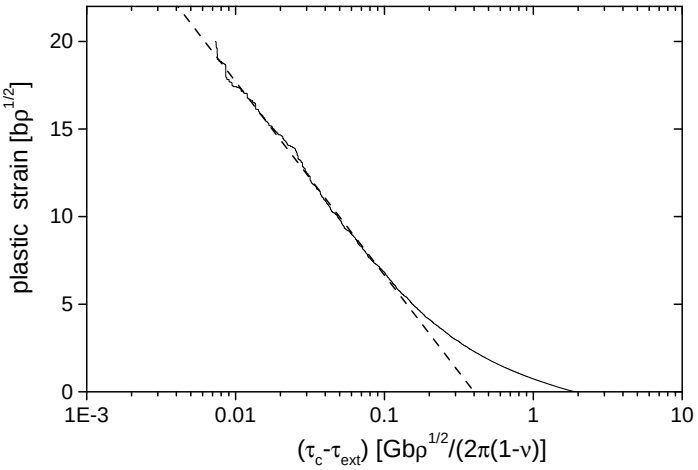

Figure 5. Ensemble-averaged stress-strain graph as obtained by averaging over 60 simulations of systems with 128 × 128 sites. Strain is plotted against distance from the critical stress.

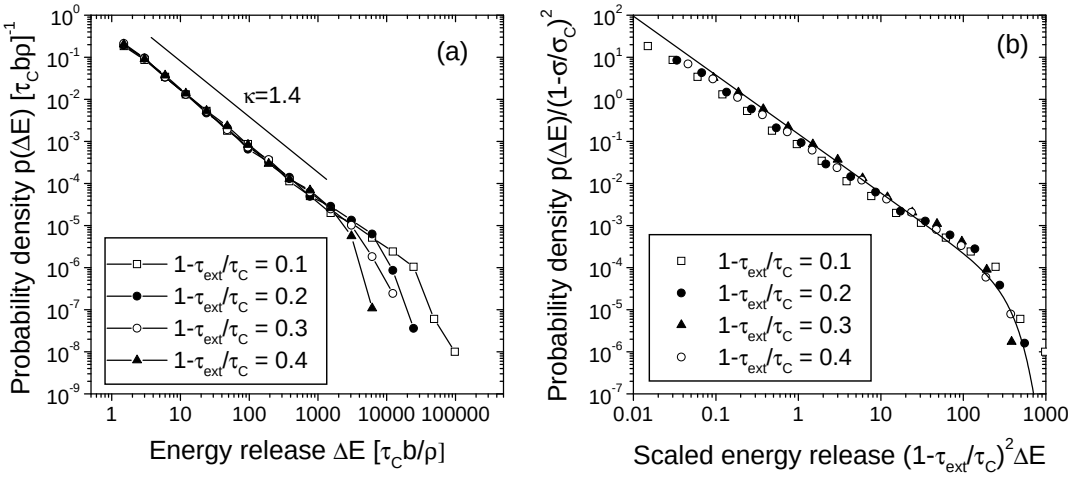

Figure 6. Probability distributions of slip avalanche sizes (probability density $p(\Delta E)$ vs. energy release ΔE) as obtained from an ensemble of systems of size 256×256. Left: distributions corresponding to different stresses; Right: universal distribution obtained by re-scaling $\Delta E \to \Delta E(1-\tau_{\rm ext}/\tau_{\rm c})^2$; full line: theoretical curve (Eq. 23).

Accordingly, the stress susceptibility $\chi = \partial\gamma/\partial\tau_{\rm ext}$ of the plastic strain diverges according to

$$\chi \propto (\tau_{\rm c} - \tau_{\rm ext})^{-\theta}\ ,\ \theta \approx 1\ . \tag{22}$$

We now investigate in more detail the 'strain bursts' that manifest themselves as stepwise strain increments in the individual stress-strain graphs. To this end, we record the strain increments (if any) which occur after each stress increment $\Delta\tau_{\rm ext}$. Since the total strain increment due to a slip avalanche depends on the system size $V_{\rm S}$ (a given local slip avalanche produces a smaller total strain increment $\Delta\gamma$ in a larger system), we characterize the avalanche sizes in terms of the dissipated energy $\Delta E = \tau_{\rm ext}\Delta\gamma V_{\rm S}$ which is proportional to the strain increment but does not depend on system size. We then determine the probability distribution of avalanche sizes within different external stress intervals, corresponding to different distances from the critical stress $\tau_{\rm c}$. Results are given in Figure 6.

The distributions exhibit a power-law decay $p(\Delta E) \propto \Delta E^{-\kappa}$ which is truncated at a characteristic avalanche size ΔE_c. As the stress approaches the critical stress τ_c, this upper limit and hence the average avalanche size diverge. Distributions obtained at different applied stresses τ_{ext} can be collapsed into a single universal distribution if the energy releases are re-scaled by a factor $(1 - \tau_{ext}/\tau_c)^{1/\sigma}$ where $\sigma \approx 0.5$ (Figure 6, right). The results for the susceptibility and the avalanche statistics are not independent since the susceptibility is proportional to the average avalanche size. We therefore expect it to diverge like $\chi \propto (\tau_c - \tau)^{-(2-\kappa)/\sigma}$. With $\kappa \approx 1.4$ and $\sigma \approx 0.5$ we find $\theta = (2 - \kappa)/\sigma \approx 1$ in agreement with Eq. (22). The exponents κ, θ and σ can be understood in terms of mean-field depinning [see e.g. Fisher (1998) or Zapperi et al. (1998)], as the theoretical values $\theta = 1, \sigma = 0.5$ and $\kappa = 1.5$ are in good agreement with the present simulation results. The theoretically predicted avalanche size distribution for mean-field depinning is

$$p(\Delta E) \propto \Delta E^{-1.5} \exp\left[-\left(\frac{\Delta E}{\Delta E_c}\right)^2\right] , \tag{23}$$

which again compares well with the results of the simulations (Figure 6).

4.2. Influence of hardening

To introduce hardening with non-dimensional hardening coefficient Θ into our model, we use two approaches: (i) We increase the amplitude of the internal-stress fluctuations (i.e., the width of the probability distribution of $\delta\tau$) in proportion with the local strain by an amount of $\Theta\gamma/\tau_c(\Theta = 0)$; (ii) We leave the width of the distribution unchanged but shift the mean value by an amount $\Theta\gamma$ that is again proportional to the local strain. Both methods result in stress-strain graphs similar to those depicted in Figure 7: The asymptotic behavior changes, as the horizontal tangent of the stress-strain graph is replaced by a tangent with slope Θ. To give again a 'feeling' for the orders of magnitude involved, we note that the simulated hardening rates correspond, with the parameters for Cu given above, to dimensional hardening rates of

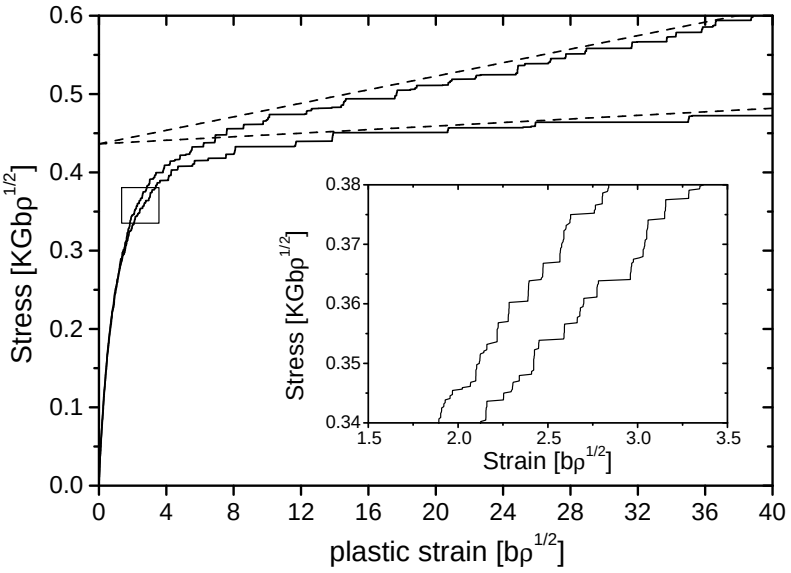

Figure 7. Stress-strain curves as in Figure 4 for hardening coefficients $\Theta = 0.001$ and $\Theta = 0.004$; dashed lines: curves $\tau = \tau_c + \Theta\gamma$ with $\tau_c = 0.44$.

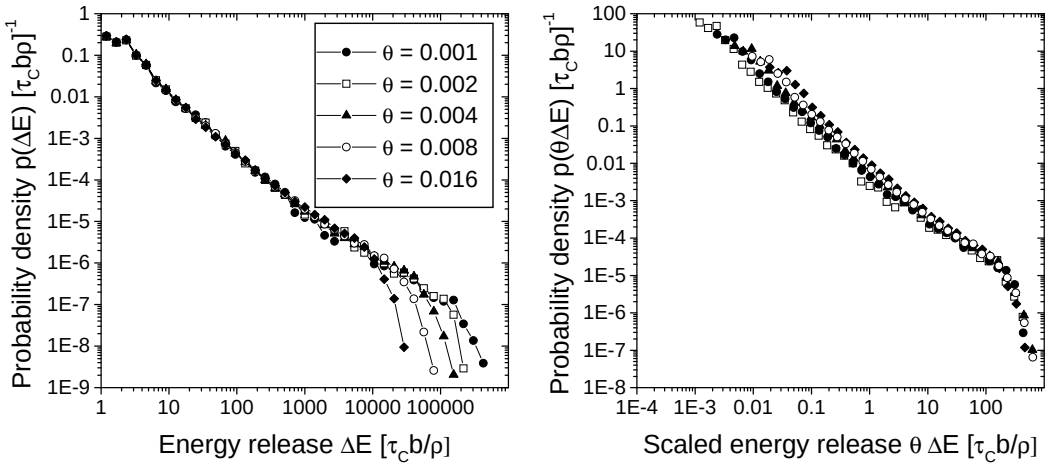

Figure 8. Probability distributions of slip avalanche sizes (probability density $p(\Delta E)$ vs. energy release ΔE) as obtained from an ensemble of systems of size 256×256. Left: distributions corresponding to different hardening rates; Right: universal distribution obtained by re-scaling $\Delta E \to \Theta \Delta E$

40 and $200MPa$ which are in the range of what is typically observed in hardening stages I and II of Cu single crystals.

It is seen from Figure 7 that the influence of hardening does not change the stepwise morphology of the stress-strain curves but eliminates the largest strain bursts which, in a non-hardening system, occur at stresses close to the critical stress. To quantify this idea, we study the avalanche statistics (evaluated for stresses above the critical stress of the non-hardening system) for different hardening rates. Figure 8 shows that the hardening does not change the power-law regime of the burst size distribution but decreases the cut-off value, which turns out to be inversely proportional to the hardening rate.

This can be easily understood from a scaling argument. The burst energy is proportional to the strain produced in a burst, and with an avalanche exponent of $\kappa \approx 1.5$ it follows that the average strain $\Delta\gamma$ follows the relation $\langle \Delta\gamma \rangle \propto \langle \Delta E \rangle \propto \Delta E_{\max}^{1/2}$. Due to hardening, each burst raises the critical stress by a small amount $\Delta\tau_c \propto \Theta \langle \Delta\gamma \rangle$, which implies that the external stress (which cannot instantaneously follow) lags behind the current critical stress by a similar amount. Finally, the maximum burst size follows the scaling relationship $\Delta E_{\max} \propto \Delta\tau^{-2}$. Combining these relations, it follows directly that $\Delta E_{\max} \propto 1/\Theta$.

4.3. Slip pattern and surface morphology

As shown in the previous sections, mean-field depinning provides a framework for understanding the size distribution of slip avalanches and the behavior of the stress-strain curves as one crosses the microplastic region and approaches the yield stress, as well as for assessing the influence of strain hardening. However, mean-field considerations can in principle not account for the observed anisotropic spatial distribution of slip, the formation of slip lines, and the development of a self-affine surface morphology. However, our simulations indicate that, owing to the particular properties of the elastic kernel, such features naturally emerge from the dynamics of our model.

Figure 9 shows a grey-scale representation of the slip pattern $\gamma(x, y)$ that emerges in a typical simulation. One observes a 'slip-line'-pattern with pronounced correlations along the

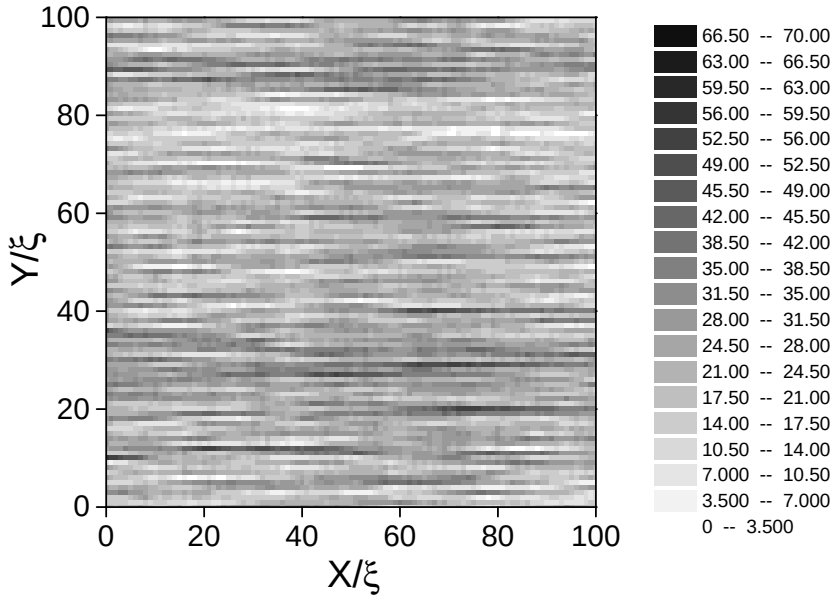

Figure 9. Strain pattern obtained after simulation of a system of size 256×256 to an average strain of $20b\sqrt{\rho}$ (slip direction from left to right); parameters as in Figure 4; greyscale: local strain in units of $b\sqrt{\rho}$

direction of slip (x direction in Figure 9). Such stratified slip patterns are commonly observed in deformation of single-slip oriented single crystals. They are considered to be a natural consequence of the directed glide of lattice dislocations along the slip planes. The present model produces 'slip-line' patterns without explicitly accounting for the motion of lattice dislocations. This is can be understood by noting that according to Eq. (13)) heterogeneities of slip in the direction of the slip plane normal (the y direction) do not give rise to any long-range stresses. Heterogeneities in the slip direction (the x direction), on the other hand, are penalized by the gradient-dependent stress contribution in Eq. (20) which tends to homogenize deformation in the slip direction. Because of these properties of the interactions, the 'manifold' $\gamma(x, y)$ is prone to fall apart in the y direction, leading to the striated deformation patterns seen in Figure 9.

We now evaluate the surface profiles which correspond to the simulated slip patterns. We consider a surface running along the plane $x = 0$. The displacement u in the direction normal to the surface fulfils the relationship

$$\frac{\partial u}{\partial y} = \gamma(x = 0, y) \; . \tag{24}$$

This can be understood as the sum of a displacement due to the average strain $\langle\gamma\rangle$, which leads to a rigid rotation of the surface, plus a random displacement due to the strain fluctuation $\delta\gamma(x = 0, y) = \gamma(x = 0, y) - \langle\gamma\rangle$. The surface profile may be obtained by direct integration of the strain fluctuation,

$$h(y) = \int_0^y [\gamma(x = 0, y') - \langle\gamma\rangle] \mathrm{d}y' \; . \tag{25}$$

A surface profile obtained in this manner is shown in Figure 10.

To assess simulated profiles in terms of their roughness exponent, we plot the mean square height difference $\langle|u(x) - u(x + l)|\rangle$ between two points along the profile as a function of their separation l. For a self-affine profile we expect $\langle|u(x) - u(x + l)|\rangle \propto l^H$ where H is the Hurst

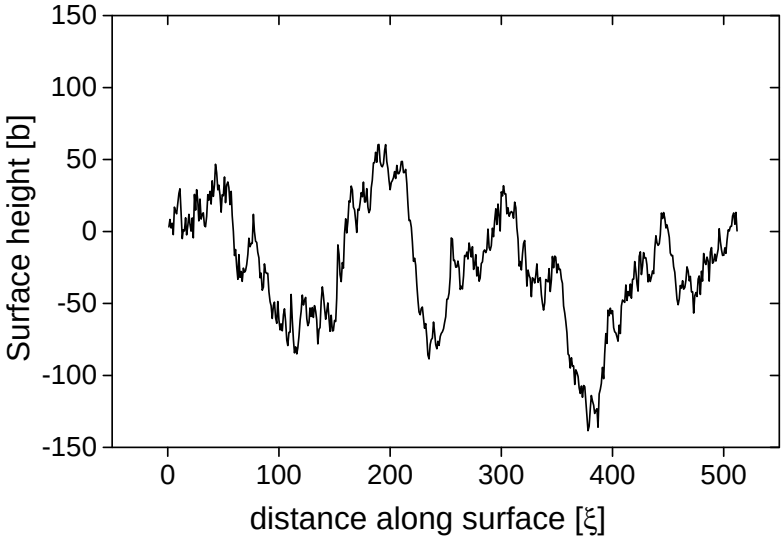

Figure 10. Surface profile obtained from a system of size 512×512 after simulation to an average strain of $\bar{\gamma} = 20b\sqrt{\rho}$.

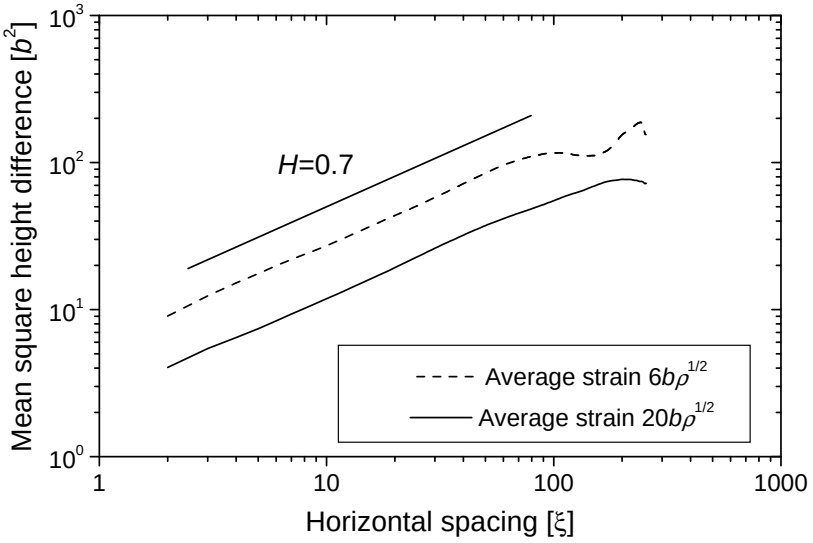

Figure 11. Mean square height difference vs. horizontal distance for surface profiles obtained from a system of size 512×512 after simulation to average strains of $6b\sqrt{\rho}$ and $20b\sqrt{\rho}$; each graph has been averaged over 10 simulated profiles.

exponent. Figure 11 demonstrates that our simulated profiles can be characterized by a Hurst exponent $H \approx 0.7$. Increasing the total strain leads to an increase in the absolute magnitude of surface height variations but does not change the value of H. Both the numerical value of the Hurst exponent and its strain independence compare well with the experimental observations quoted in the introduction.

5. Conclusions

Our simulations demonstrate that it is possible to capture essential aspects of slip avalanches in terms of a simple continuum model. By combining a fluctuating local stress-strain relationship

with a strain-gradient dependent stress contribution and long-range stresses mediated by the elastic Green's function, the model accounts both for the observed spatial heterogeneities of plastic deformation (slip lines, self-affine surface roughness) and the emergence of 'bursts' of plastic activity with a power-law size distribution.

The present model has a fairly generic formal structure, and many of our qualitative results do not depend critically on the particular physical assumptions made. For instance, it is not crucial to relate the fluctuating flow stress to the stress fluctuations associated with a homogeneous distribution of dislocations as done in Section 2.3. Concepts of randomness and disorder also apply to flow stress fluctuations arising from other types of random microstructure such as irregular patterns of dislocation cells, or from the statistical activation and exhaustion/blocking of dislocation sources. However, there are still several crucial questions that need to be studied: (i) Is it possible to formulate a dislocation-based model which exhibits the same behavior as the present phenomenological continuum model? (ii) How does the behavior of the model change if we allow for slip on multiple slip systems, such that the tensorial nature of the plastic strain becomes important? (iii) What is the influence of surface boundary conditions on the slip patterns – are the simulated 'surface profiles' truly equivalent to those emerging on a free surface, where the stresses are by necessity different from the bulk?

In general terms, or results indicate that fluctuation phenomena in plastic flow of crystalline solids can be envisaged as critical phenomena in driven non-equilibrium systems. The theory of elastic interface depinning provides a theoretical framework which covers a wide range of phenomena including avalanche dynamics in the motion of magnetic domain walls (Barkhausen noise, Zapperi et al. 1998), the dynamics of earthquakes or the motion of cracks (Fisher, 1998). The present model adopts this framework to problems of plastic flow. An analogous effort has been made in relation with the plasticity of amorphous materials by Baret et al. (2002). Peculiarities arise in the present case from the particular deformation geometry: In a crystalline solid deforming in single slip, where deformation is restricted to simple shear occurring along a single set of planes, the elastic kernel which mediates long-range elastic interactions is not positively definite. The consequences of this observation as well as the reasons for the emergence of a power-law decay of correlations in the strain pattern (which has, to the knowledge of the authors, not been observed in other depinning-type models) remain to be assessed in future work.

Acknowledgements

Financial support by the European Commission under RTN/SizeDepEn HPRN-CT 2002-00198 and of EPSRC under Grant No. GR/S20406/01 is gratefully acknowledged. We also thank Mikko Alava and Stefano Zapperi for many stimulating discussions on problems of interface depinning.

References

Baret, J.-C., Vandembroucq, D., Roux, S., 2002. An extremal model for amorphous media plasticity. Phys. Rev. Lett. 89, 195506.

Chen,K., Bak, P., Obukhov, S.P., 1991. Self-organized criticality in a crack-propagation model of earthquakes. Phys. Rev. A 43, 625-630.

Fisher, D.S., 1998. Collective transport in random media: From superconductors to earthquakes. Phys. Rep. 301, 113-150.

Groma, I., Bako, B., 1998. Probability distribution of internal stresses in parallel straight dislocation systems. Phys. Rev. B 58, 2969-2974.

Groma, I., Csikor, F., and Zaiser, M., 2003. Spatial correlations and higher-order gradient terms in a continuum description of dislocation dynamics. Acta Mater. 51, 1271-1281.

Middleton, A.A., 1992. Asymptotic uniqueness of the sliding state for charge-density waves. Phys. Rev. Lett. 68, 670-673.

Miguel, M.C., Vespignani, A., Zapperi, S., Weiss, J., Grasso, J.-R., 2001. Intermittent dislocation flow in viscoplastic deformation. Nature 410, 667-671.

Neuhäuser, H., 1984. Slip-line formation and collective dislocation motion. In: F.R.N. Nabarro (Ed.), Dislocations in Solids, Vol. 4, North-Holland, Amsterdam, pp. 319-440.

Weiss, J., Grasso, J.-R., 1997. Acoustic emission in Single Crystals of Ice. J. Phys. Chem. B 101, 6113-6117.

Weiss, J., Marsan, D., 2003. Three-dimensional mapping of dislocation avalanches: Clustering and space/time coupling. Science 299, 89-92.

Uchic, M.D., Dimiduk, D.M., Florando, J.N., and Nix, W.D., 2004. Sample Dimensions Influence Crystal Strength and Plasticity. Science 305, 986-989.

Zaiser, M., 1998. A generalized composite approach to the flow stress and strain hardening of crystals containing heterogeneous dislocation distributions. Materials Science and Engineering A 249, 145-151.

Zaiser, M., Miguel, M.-C, Groma, I., 2001. Statistical dynamics of dislocation systems: The influence of dislocation-dislocation correlations. Phys. Rev. B 64, 224102.

Zaiser, M., Seeger, A., 2002. Long-range internal stresses, dislocation patterning and work hardening in crystal plasticity. In: F.R.N. Nabarro and M.S. Duesbery (Eds.), Dislocations in Solids, Vol. 11, North-Holland, Amsterdam, pp. 1-100.

Zaiser, M., Madani F., Koutsos, V., Aifantis E.C., 2004. Self-affine surface morphology of plastically deformed metals. Phys. Rev. Letters 93, 195507.

Zaiser, M., Aifantis, E.C., 2005. On the theory of gradient plasticity III: Random effects and slip avalanches, Int. Journal of Plasticity (in press).

Zapperi, S., Cizeau, P., Durin, G., Stanley, H.E., 1998. Dynamics of a ferromagnetic domain wall - Avalanches, depinning and the Barkhausen effect. Phys. Rev. B 58, 6353-6366.